Selective Catalytic Chemistry at Rhodium(II) Nodes in Bimetallic Metal–Organic Frameworks

Deependra M. Shakya, Otega A. Ejegbavwo, Thayalan Rajeshkumar, Sanjaya D. Senanayake, Amy J. Brandt, Sharfa Farzandh, Narayan Acharya, Amani M. Ebrahim, Anatoly I. Frenkel, Ning Rui, Gregory L. Tate, John R. Monnier, Konstantinos D. Vogiatzis,* Natalia B. Shustova,* and Donna A. Chen*

Abstract: *We report the first study of a gas-phase reaction catalyzed by highly dispersed sites at the metal nodes of a crystalline metal–organic framework (MOF). Specifically, CuRhBTC (BTC³⁻ = benzenetricarboxylate) exhibited hydrogenation activity, while other isostructural monometallic and bimetallic MOFs did not. Our multi-technique characterization identifies the oxidation state of Rh in CuRhBTC as +2, which is a Rh oxidation state that has not previously been observed for crystalline MOF metal nodes. These Rh^{2+} sites are active for the catalytic hydrogenation of propylene to propane at room temperature, and the MOF structure stabilizes the Rh^{2+} oxidation state under reaction conditions. Density functional theory calculations suggest a mechanism in which hydrogen dissociation and propylene adsorption occur at the Rh^{2+} sites. The ability to tailor the geometry and ensemble size of the metal nodes in MOFs allows for unprecedented control of the active sites and could lead to significant advances in rational catalyst design.*

The use of crystalline metal–organic frameworks (MOFs) as heterogeneous catalysts provides the unique opportunity to tailor active site geometries and ensemble sizes on the atomic scale. MOFs are crystalline hybrid inorganic/organic materials with structures consisting of metal nodes of specific geometries connected by organic linkers. Furthermore, the high porosity (> 1000 m²g⁻¹ surface area)[1] of MOFs provides a sufficient number of highly dispersed active sites for catalytic reactions.

MOFs are reported to be excellent catalysts for a number of reactions in the liquid phase, including hydrogenation, oxidation, and epoxidation.[2] However, gas-phase heterogeneous catalysis is preferred over reactions in the liquid phase due to the ease of separating the catalyst from the products in the former case. Given their extraordinarily high surface areas, MOFs have been used as supports for metal particles in gas phase reactions.[3] Similarly, catalytically active metal complexes or clusters have been coordinated to the MOF nodes or linkers by postsynthetic modification.[4] In comparison to these catalysts that employ the MOF as a support, the use of metal nodes intrinsic to the MOF structure as the catalytically active sites has several advantages. These include: a homogeneous distribution of the metal nodes within the framework; and a well-defined structure of the metal nodes, which can be fully characterized by crystallography and can be investigated theoretically to predict the possible mechanisms of catalytic transformations.

In this work, we present the first study of gas-phase catalytic activity occurring at the metal nodes of a crystalline MOF and investigate possible reaction mechanisms using density functional theory (DFT) calculations. Specifically, $(Cu_xRh_{1-x})_3(BTC)_2$ (abbreviated CuRhBTC, where BTC³⁻ = benzenetricarboxylate) is found to catalyze propylene hydrogenation to propane with relatively high activity and excellent long-term stability, whereas the other bimetallic and monometallic MOFs investigated exhibit no activity. CuRhBTC is prepared via solid-state metathesis using $Cu_3(BTC)_2$ (HKUST-1) as a precursor. To the best of our knowledge, this is the first report of a +2 oxidation state for isolated Rh ions in a MOF; these Rh^{2+} ions are not stabilized by the presence of Rh–Rh bonds at Rh dimer nodes,[5] and are produced through the reduction of postsynthetically incorporated Rh³⁺. This unusual Rh^{2+} oxidation state provides the active sites for the reaction, given that activity increases with Rh concentration. DFT studies were used to model the active Rh^{2+} sites within the CuRhBTC structure and to identify an energetically favorable reaction mechanism in which H_2 dissociation and propylene adsorption occur at Rh^{2+} sites.

Propylene hydrogenation experiments were carried out on the monometallic CuBTC and NiBTC MOFs, as well as a variety of Cu-containing bimetallic MOFs $((Cu_xM_{1-x})_3$-

[*] D. M. Shakya, O. A. Ejegbavwo, Dr. A. J. Brandt, S. Farzandh,
N. Acharya, Prof. N. B. Shustova, Prof. D. A. Chen
Department of Chemistry and Biochemistry, University of South
Carolina, Columbia, SC 29208 (USA)
E-mail: shustova@sc.edu
         dachen@sc.edu

Dr. T. Rajeshkumar, Prof. K. D. Vogiatzis
Department of Chemistry, University of Tennessee
Knoxville, TN 37996 (USA)
E-mail: kvogiatz@utk.edu

Dr. S. D. Senanayake, Prof. A. I. Frenkel, Dr. N. Rui
Chemistry Division, Brookhaven National Laboratory
Upton, NY 11973 (USA)

A. M. Ebrahim, Prof. A. I. Frenkel
Department of Materials Science and Chemical Engineering, Stony
Brook University, Stony Brook, NY 11794 (USA)

G. L. Tate, Prof. J. R. Monnier
Department of Chemical Engineering, University of South Carolina
Columbia, SC 29208 (USA)

Supporting information and the ORCID identification number(s) for
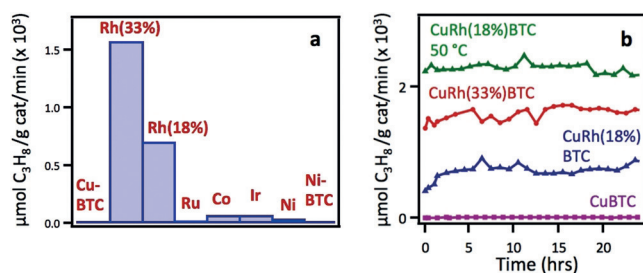the author(s) of this article can be found under https://doi.org/10.
1002/anie.201908761.

Figure 1. a) Average propylene hydrogenation activity for the following bimetallic CuMBTC and monometallic MBTC MOFs at 20°C: CuBTC, CuRh(33%)BTC, CuRh(18%)BTC, CuRu(6%)BTC, CuCo(50%)BTC, and CuIr(5%)BTC; and at 100°C: CuNi(6%)BTC and NiBTC; and b) activity for propylene hydrogenation as a function of time on stream over CuRhBTC with the following Rh concentrations: 18% Rh at 20°C and 50°C; 33% Rh at 20°C; and 0% Rh (pure CuBTC) at 20°C.

(BTC)$_2$) where M = Rh, Co, Ni, Ir and Ru, as shown in Figure 1a. Only the CuRhBTC exhibited significant activity for propane production at 20°C ($\approx$1600 µmol g cata-catalyst^{-1} min^{-1} for CuRh(33%)BTC). Specifically, the pure CuBTC MOF showed no activity under the same reaction conditions, indicating that the Cu^{2+} ions are not active for propylene hydrogenation. Pure NiBTC also had no appreciable hydrogenation activity. Note that monometallic RhBTC was not studied due to its loss of crystallinity upon exposure to air, and the instability of RhBTC is attributed to the fact that the paddle-wheel configuration of the metal nodes is highly strained for Rh ions.[6] For all MOF catalysts, powder X-ray diffraction (PXRD) data were collected immediately after reaction, and catalysts exhibited the same high crystallinity observed before reaction.

The activity of the CuRh(33%)BTC catalyst is also stable over a 24 hour period on stream (Figure 1b). Moreover, CuRhBTC with a lower bulk concentration of Rh (18%) has 45% of the activity of the CuRh(33%)BTC, which indicates that activity scales with Rh concentration and suggests that the Rh ions are the active sites for reaction. At 50°C, the reaction rate for CuRh(18%)BTC is 3.2 times higher than at 20°C and is stable over the entire period on stream. The apparent activation energy for propylene hydrogenation on CuRhBTC was determined to be 6.3 kcal mol^{-1} based on data collected at 20–50°C (Figure S1 in the Supporting Information).

X-ray photoelectron spectroscopy (XPS) experiments address the oxidation state of the Rh ions in CuRhBTC (Figure 2). For the as-prepared sample, the Rh(3d$_{5/2}$) peak has a binding energy of 309.2 eV. The spectrum of dirhodium (II) tetraacetate (Rh$_2$(OAc)$_4$) provides a standard for the relatively uncommon Rh^{2+} oxidation state, which appears at 308.9 eV for Rh$_2$(OAc)$_4$ and is similar to the value observed for CuRhBTC. Furthermore, the Rh(3d) spectra for highly dispersed Rh^{2+} ions prepared from incipient wetness impregnation of Rh$_2$(OAc)$_4$ on silica shows identical binding energies and peak widths to that of CuRhBTC; therefore the relative broadness of the Rh(3d$_{5/2}$) peak for CuRhBTC cannot be attributed to mixed oxidation states since Rh$_2$-(OAc)$_4$/SiO$_2$ is equally broad and contains only Rh^{2+}. In contrast, Rh^{3+} in RhCl$_3$ appears at 310.1 eV, which is
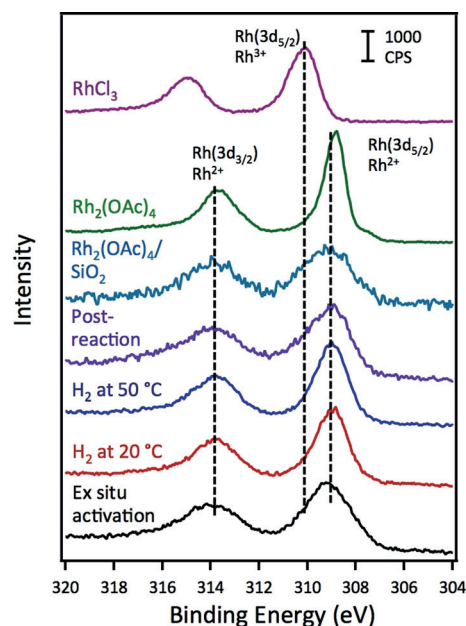

Figure 2. X-ray photoelectron spectroscopy data for the Rh(3d) region for the CuRh(33%)BTC MOF: after activation by heating at 160°C in vacuo for 24 hours; after exposure to flowing H$_2$ at room temperature for 2 hours; after heating in flowing H$_2$ at 50°C for 2 hours; and after propylene hydrogenation at 20°C and 50°C in the reactor (MOF catalyst from Figure 1). Spectra for a Rh$_2$(OAc)$_4$/SiO$_2$ catalyst prepared by incipient wetness impregnation ($\times$7), crystalline Rh$_2$(OAc)$_4$ ($\times$0.5) and RhCl$_3$ ($\times$0.5) are shown for comparison of binding energies.

consistent with Rh^{3+} oxidation states reported in the literature,[7] whereas Rh^{1+} is expected at 308.0–308.4 eV.[7,8] There is no evidence for metallic Rh at 307.0–307.4 eV in the spectrum of CuRhBTC.[7,9] In addition, the Rh^{2+} ions in CuRhBTC are stable under reducing conditions since exposure of CuRhBTC to flowing H$_2$ at room temperature and 50°C results in almost no change in binding energy. The nearly identical Rh(3d) peak shapes for the as-prepared MOF and the post-reaction catalyst used for the hydrogenation experiment in Figure 1 are also consistent with a stable Rh^{2+} oxidation state during reaction.

The X-ray absorption near edge structure (XANES) data provide further evidence for the assignment of the Rh^{2+} oxidation state in CuRhBTC. As shown in Figure 3, the Rh
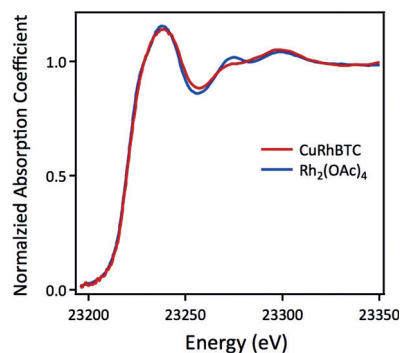

Figure 3. Rh K-edge XANES data for CuRhBTC and Rh$_2$(OAc)$_4$.

K-edge is nearly identical for CuRhBTC and the Rh$_2$(OAc)$_4$, which has an oxidation state of +2. In contrast, the Rh K-edges for RhCl$_3$ and [Rh^I(CO)$_2$Cl]$_2$ have distinctly different XANES features compared to those in the CuRhBTC spectrum (Figure S2a). The Cu K-edge for CuRhBTC is identical to that for CuBTC; a comparison with the spectrum of Cu^{II} oxide indicates that the Cu oxidation state in CuRhBTC is consistent with Cu^{2+}, whereas the Cu^I oxide and metallic Cu^0 standards exhibit different spectra (Figure S2b). EXAFS data were also collected and analyzed for the Cu and Rh K-edges to provide complementary information to the XANES experiments (see Supporting Information).

Ambient pressure (AP)-XPS studies establish that the Rh oxidation state in CuRhBTC does not change during exposure to the reactant gases or pure H$_2$. Figure 4 shows the
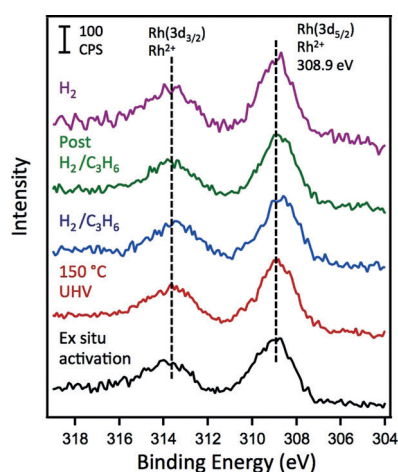

Figure 4. X-ray photoelectron spectroscopy data for the Rh(3d) region for CuRhBTC: after pumping down in the UHV chamber; after heating at 150°C in UHV for 1.5 hours; during exposure to 32 mTorr H$_2$/ 8 mTorr propylene at room temperature; in UHV after exposure to H$_2$/ propylene; and during exposure to 20 mTorr H$_2$ at room temperature.

Rh(3d) region for the CuRhBTC and this same sample: after activation by heating at 150°C for 1.5 hours in ultrahigh vacuum (UHV); during exposure to 32 mTorr H$_2$/8 mTorr propylene at room temperature; and in UHV following the H$_2$/propylene exposure. The Rh(3d) spectrum collected during exposure to 20 mTorr H$_2$ is also shown for another CuRhBTC sample that was initially activated at 150°C in UHV. In all cases, the Rh(3d) spectra exhibit no appreciable change in peak shape or binding energy, implying that the Rh oxidation state remains Rh^{2+} under all conditions, and this behavior is also consistent with the Rh(3d) spectrum of the post-reaction CuRhBTC (Figure 2).

Both the XPS and AP-XPS studies demonstrate that the CuRhBTC contains Cu^{2+} as the main species although Cu^{1+} is also present (Figure S3: Cu(2p), Cu AES and C(1s) regions). Previous studies by our group have established that reduction of Cu^{2+} to Cu^{1+} in pure CuBTC is induced by the combination of X-ray irradiation and heating to remove coordinating solvent molecules.[10] The fact that the post-reaction CuRhBTC exhibits a Cu(2p$_{3/2}$) peak identical to that of the

pre-reaction MOF suggests that there is no change in oxidation state of the Cu ions after propylene hydrogenation (Figure S3). Moreover, exposure of CuRhBTC to H$_2$ at room temperature does not cause significant reduction of Cu^{2+}. Consequently, there is no direct evidence that reduction of Cu^{2+} plays a role in propylene hydrogenation, particularly since CuBTC, which also contains both Cu^{1+} and Cu^{2+}, is inactive for propylene hydrogenation.

In order to understand the intrinsic activity of the Rh^{2+} site, propylene hydrogenation was also studied on dirhodium-(II) tetraacetate (Rh$_2$(OAc)$_4$); this species served as a molecular model for the pure Rh paddle-wheel node. At 20°C, crystalline Rh$_2$(OAc)$_4$ exhibits stable hydrogenation activity (11000 µmol g cat^{-1} min^{-1}), which confirms that Rh^{2+} ions provide the active sites (Figure S4a). The apparent activation energy for the Rh$_2$(OAc)$_4$ catalyst determined from activity measurements at 0–40°C is 5.4 kcal mol^{-1} (Figure S4b), which is a value similar to that of CuRhBTC and suggests a common mechanism. Hydrogenation activity for Rh^{2+} is consistent with reports in the literature for Rh$_2$(OAc)$_4$,[11] as well as for Rh^{2+} ions in amorphous coordination polymers containing dinuclear rhodium paddle-wheel units.[6,12] However, the Rh^{2+} active site in Rh$_2$(OAc)$_4$ is unstable under reaction conditions, in contrast to the high stability of Rh^{2+} in CuRhBTC. Specifically, Rh$_2$(OAc)$_4$ is reduced to metallic Rh after exposure to H$_2$ at 50°C (Figure S5), and the unstable propylene hydrogenation activity for Rh$_2$(OAc)$_4$ at 50°C (Figure S4a) is attributed to reduction of Rh^{2+} to metallic Rh, as confirmed by post-reaction XPS and XRD studies.

Hydrogenation activity of the CuRhBTC cannot be attributed to the presence of residual Rh^{3+} ions retained in the MOF pores after exposure to RhCl$_3$ during ion exchange because RhCl$_3$ itself has no activity for propylene hydrogenation at 20°C (Figure S6). Furthermore, Rh^{3+} becomes reduced at 50°C under hydrogenation conditions, as demonstrated by the activity data as well as XPS data for RhCl$_3$ exposed to H$_2$ at 50°C. Further discussion of the Rh^{3+} activity is presented in the Supporting Information.

In order to better understand propylene hydrogenation on CuRhBTC, DFT studies were carried out to investigate the reaction mechanism. All calculations were performed with the Gaussian09 program package[13] using the M06-L[14] functional and the def2-TZVPP[15] basis set (see Supporting Information). The full reaction profile for propylene hydrogenation catalyzed by the bimetallic CuRh node of CuRhBTC is shown in Figure 5. Table S1 provides relative energy differences for the intermediates and transition states with respect to the CuRh node and the reactants, as well as key bond distances that demonstrate the evolution of the reaction.

The first step in the reaction mechanism is the coordination of propylene at the open site of the Rh^{2+} cation (intermediate **1**) via π-backbonding; propylene adsorbs more strongly than H$_2$ at Rh^{2+} sites by ≈13 kcal mol^{-1} (see Supporting Information). In intermediate **1**, Rh can be considered as a hexacoordinated metal after accounting for a weak bond with the Cu^{2+} cation (see Supporting Information), and therefore the mechanism for H$_2$ dissociation is not obvious. Several possible mechanisms were considered,
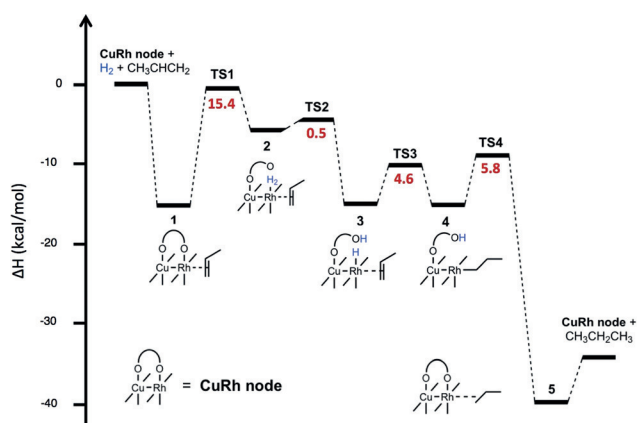
Figure 5. Reaction profile for propylene hydrogenation catalyzed at the bimetallic CuRh node of CuRhBTC.

including H_2 dissociation on pentacoordinated Rh^{2+} and direct H-transfer to propylene for the formation of a propyl radical (see Supporting Information). However, the lowest energy pathway for H_2 dissociation involves cleavage of the Rh−O bond to create a second vacant site in the coordination sphere of Rh^{2+} for the binding of H_2. Although this step has a relatively high activation energy, the decoordinated oxygen atom facilitates H_2 dissociation in the next step via the formation of OH.[16] Furthermore, the reaction barrier for H_2 dissociation is only 0.5 kcal mol^{-1} (**TS2**) and leads to the thermodynamically more stable intermediate **3**. After the H_2 bond is cleaved, a Rh monohydride and a hydroxyl group are formed. Next, the hydrogen atom of the Rh-hydride is transferred to propylene (**TS3**) to form the Rh-propyl intermediate **4**. Finally, a second hydrogen atom from the hydroxyl group is transferred to the propyl radical (**TS4**) for the formation of the final product. The desorption of propane and reformation of the Rh−O bond close the catalytic cycle. Note that the activation energy barrier for Rh−O bond dissociation (≈ 15 kcal mol^{-1}) is higher than the experimentally measured activation energy of 6.3 kcal mol^{-1}. A possible explanation for this discrepancy is that CuRhBTC serves as a pre-catalyst, where species **2** provides the active sites, and the Rh−O bond is not reformed in the catalytic cycle. In that case, addition of hydrogen to adsorbed propyl would be the rate-limiting step, and the calculated barrier of 5.8 kcal mol^{-1} agrees well with the experimental value. This hypothesis will be further discussed in a subsequent publication. Investigations were also conducted on $Rh_2(OAc)_4$ as a model system for addressing activity at monometallic Rh^{2+} sites, and a similar mechanism for reaction on $Rh_2(OAc)_4$ is reported in Figure S7.

Spin density plots for the CuRh node of CuRhBTC (Figures S8 and S9) demonstrate the lack of significant overlap between the half-filled $4d_z$ orbital on Rh^{2+} and the half-filled $3d_{x2-y2}$ on Cu^{2+}. These results suggest minimal electronic interaction between the two metal centers, but a more detailed investigation of the bimetallic interactions and their role in the reaction is the topic of an ongoing study.

In summary, this study represents the first report of gas-phase catalysis at the metal nodes of a crystalline MOF, as well as the first report of Rh^{2+} MOF nodes prepared via the reduction of postsynthetically incorporated Rh^{3+}. Propylene hydrogenation activity at room temperature is observed for CuRhBTC, whereas CuBTC itself and CuMBTC (M = Co, Ir, Ni, Ru ions) have no appreciable activity, thus illustrating the unique hydrogenation activity of Rh^{2+} in the CuBTC framework. The Rh^{2+} ions in the bimetallic MOF structure are stable under reaction conditions for up to 24 hours and are essential for the reaction pathways, as demonstrated by DFT calculations. The main role of the Cu ions in CuRhBTC is believed to be the stabilization of the MOF framework, which prevents incorporated Rh^{2+} from becoming reduced to metallic Rh under reaction conditions. This work provides fundamental understanding for the rational design of MOF catalysts, which exhibit the exceptionally high selectivity typically associated with homogeneous catalysts, but are more stable under reaction conditions than their molecular analogs.

Conflict of interest

The authors declare no conflict of interest.

[1] C. Wang, D. M. Liu, W. B. Lin, *J. Am. Chem. Soc.* **2013**, *135*, 13222–13234.

[2] a) M. M. Bhasin, J. H. McCain, B. V. Vora, T. Imai, P. R. Pujado, *Appl. Catal. A* **2001**, *221*, 397–419; b) M. J. Beier, W. Kleist, M. T. Wharmby, R. Kissner, B. Kimmerle, P. A. Wright, J. D. Grunwaldt, A. Baiker, *Chem. Eur. J.* **2012**, *18*, 887–898; c) H. Furukawa, K. E. Cordova, M. O'Keeffe, O. M. Yaghi, *Science*

2013, *341*, 1230444; d) E. Miniussi, E. R. Hernandez, M. Pozzo, A. Baraldi, E. Vesselli, G. Comelli, S. Lizzit, D. Alfe, *J. Phys. Chem. C* **2012**, *116*, 23297–23307; e) P. F. Ji, K. Manna, Z. Lin, X. Y. Feng, A. Urban, Y. Song, W. B. Lin, *J. Am. Chem. Soc.* **2017**, *139*, 7004–7011.

[3] a) T. Drake, P. F. Ji, W. B. Lin, *Acc. Chem. Res.* **2018**, *51*, 2129–2138; b) M. T. Zhao, K. Yuan, Y. Wang, G. D. Li, J. Guo, L. Gu, W. P. Hu, H. J. Zhao, Z. Y. Tang, *Nature* **2016**, *539*, 76–80.

[4] a) T. Islamoglu, S. Goswami, Z. Y. Li, A. J. Howarth, O. K. Farha, J. T. Hupp, *Acc. Chem. Res.* **2017**, *50*, 805–813; b) D. Yang, S. O. Odoh, J. Borycz, T. C. Wang, O. K. Farha, J. T. Hupp, C. J. Cramer, L. Gagliardi, B. C. Gates, *ACS Catal.* **2016**, *6*, 235–247; c) K. I. Otake, Y. X. Cui, C. T. Buru, Z. Y. Li, J. T. Hupp, O. K. Farha, *J. Am. Chem. Soc.* **2018**, *140*, 8652–8656; d) Z. Li, N. M. Schweitzer, A. B. League, V. Bernales, A. W. Peters, A. Getsoian, T. C. Wang, J. T. Miller, A. Vjunov, J. L. Fulton, J. A. Lercher, C. J. Cramer, L. Gagliardi, J. T. Hupp, O. K. Farha, *J. Am. Chem. Soc.* **2016**, *138*, 1977–1982.

[5] T. R. Felthouse, *Prog. Inorg. Chem.* **1982**, *29*, 73–166.

[6] G. Nickerl, U. Stoeck, U. Burkhardt, I. Senkovska, S. Kaskel, *J. Mater. Chem. A* **2014**, *2*, 144–148.

[7] R. Lang, T. B. Li, D. Matsumura, S. Miao, Y. J. Ren, Y. T. Cui, Y. Tan, B. T. Qiao, L. Li, A. Q. Wang, X. D. Wang, T. Zhang, *Angew. Chem. Int. Ed.* **2016**, *55*, 16054–16058; *Angew. Chem.* **2016**, *128*, 16288–16292.

[8] X. S. Zhou, Z. R. Dong, H. M. Zhang, J. W. Yan, J. X. Gao, B. W. Mao, *Langmuir* **2007**, *23*, 6819–6826.

[9] C. D. Wagner, W. M. Riggs, L. E. Davis, J. F. Moulder in *Handbook of X-ray Photoelectron Spectroscopy*, Perkin Elmer Corporation, Eden Prairie, MN, **1979**, pp. 108–109.

[10] A. S. Duke, E. A. Dolgopolova, R. P. Galhenage, S. C. Ammal, A. Heyden, M. D. Smith, D. A. Chen, N. B. Shustova, *J. Phys. Chem. C* **2015**, *119*, 27457–27466.

[11] B. C. Y. Hui, W. K. Teo, G. L. Rempel, *Inorg. Chem.* **1973**, *12*, 757–762.

[12] T. Sato, W. Mori, C. N. Kato, E. Yanaoka, T. Kuribayashi, R. Ohtera, Y. Shiraishi, *J. Catal.* **2005**, *232*, 186–198.

[13] M. J. Frisch, et al. Gaussian 09, Revision D.01, Gaussian, Inc. **2013**.

[14] Y. Zhao, D. G. Truhlar, *Theor. Chem. Acc.* **2008**, *120*, 215–241.

[15] F. Weigend, R. Ahlrichs, *Phys. Chem. Chem. Phys.* **2005**, *7*, 3297–3305.

[16] A. Szécsényi, G. N. Li, J. Gascon, E. A. Pidko, *Chem. Sci.* **2018**, *9*, 6765–6773.